The British Journal of Radiology, 85 (2012), 697–708

REVIEW ARTICLE

Watching tumours gasp and die with MRI: the promise of hyperpolarised ^{13}C MR spectroscopic imaging

K BRINDLE, MA, DPhil

Department of Biochemistry, University of Cambridge, Cambridge, UK

ABSTRACT. A better understanding of tumour biology has led to the development of ''targeted therapies'', in which a drug is designed to disrupt a specific biochemical pathway important for tumour cell survival or proliferation. The introduction of these drugs into the clinic has shown that patients can vary widely in their responses. Molecular imaging is likely to play an increasingly important role in predicting and detecting these responses and thus in guiding treatment in individual patients: so-called ''personalised medicine''. The aim of this review is to discuss how hyperpolarised ^{13}C MR spectroscopic imaging might be used for treatment response monitoring. This technique, which increases the sensitivity of detection of injected ^{13}C-labelled molecules by >10 000-fold, has allowed a new approach to metabolic imaging. The basic principles of the technique and its potential advantages over other imaging methods for detecting early evidence of treatment response will be discussed. Given that the technique is poised to translate to the clinic, I will also speculate on its likely applications.

Received 3 October 2011
Revised 3 January 2012
Accepted 5 January 2012

DOI: 10.1259/bjr/81120511

The challenge in oncology will be to match the patient to the drug, selecting those patients who respond to a drug and switching the treatment of those who do not. This has benefits from early phase clinical trials; for example, Avastin® (Genentech Inc., San Francisco, CA; bevacizumab) may have performed better in a carefully stratified breast cancer patient population [1] than in routine application in the clinic. In patients with non-small-cell lung cancer, sequencing of the epidermal growth factor receptor (EGFR) has identified activating mutations within the kinase domain that are associated with altered signalling and increased sensitivity to EGFR inhibitors [2]. Genome sequencing of tumour biopsies is likely, in the longer term, to play an important role in selection of the most appropriate drug or combination of drugs for individual patients [3]. However, there are some important limitations to this approach. Tumours can be genomically unstable and therefore intrinsically heterogeneous, which could bias the result of any analysis depending on when and where in the tumour the biopsy was taken [4]. Moreover, it may not always be possible to biopsy the tumour and its metastases routinely during the course of treatment, when new mutations may arise [3]. Therefore, while mutation analysis may be an important first step in patient stratification and therapy selection, imaging is likely to play an increasingly important role when treatment is under way, monitoring early regional responses of the primary tumour and its metastases and detecting possible relapse at later time points. Inevitably, cost–benefit must be considered. If a therapy costs $88 000 per annum [1], an imaging test that costs only $1000–2000 and which shows whether the treatment is working within weeks, days or even hours will clearly be cost-effective.

Currently, treatment response is still largely assessed by using imaging measurements to monitor reductions in tumour size, with the latest guidelines for Response Evaluation Criteria in Solid Tumours (RECIST, v. 1.1) defining partial therapy response as ''at least a 30% decrease in the sum of diameters of target lesions, taking as reference the baseline sum diameters'' [5]. However, this can be a slow method for detecting response, with reductions in tumour size not becoming evident for weeks or even months; in some cases, reductions may not occur at all, for example following treatment with anti-angiogenic drugs [6]. In these situations, ineffective treatments may be given, losing precious time and exposing the patient to harmful side-effects. Imaging tumour biology, however, may give a much earlier indication of treatment response than measurements of tumour size alone. This has been well demonstrated by [^{18}F]fludeoxyglucose ([^{18}F]FDG) positron emission tomography (PET) measurements of response to imatinib treatment in patients with gastrointestinal stromal tumours. PET measurements of the tumour uptake of this ^{18}F-labelled glucose analogue can show a marked reduction in glucose uptake following drug treatment, indicating that the patient is responding to treatment, despite the fact that the tumour can continue to increase in size (Figure 1) [7].

In this review, I will describe how ^{13}C MR spectroscopic imaging of tumour metabolism with hyperpolarised

Address correspondence to: Professor Kevin Brindle, Department of Biochemistry, University of Cambridge, Tennis Court Road, Cambridge CB2 1GA, UK. E-mail: kmb@mole.bio.cam.ac.uk

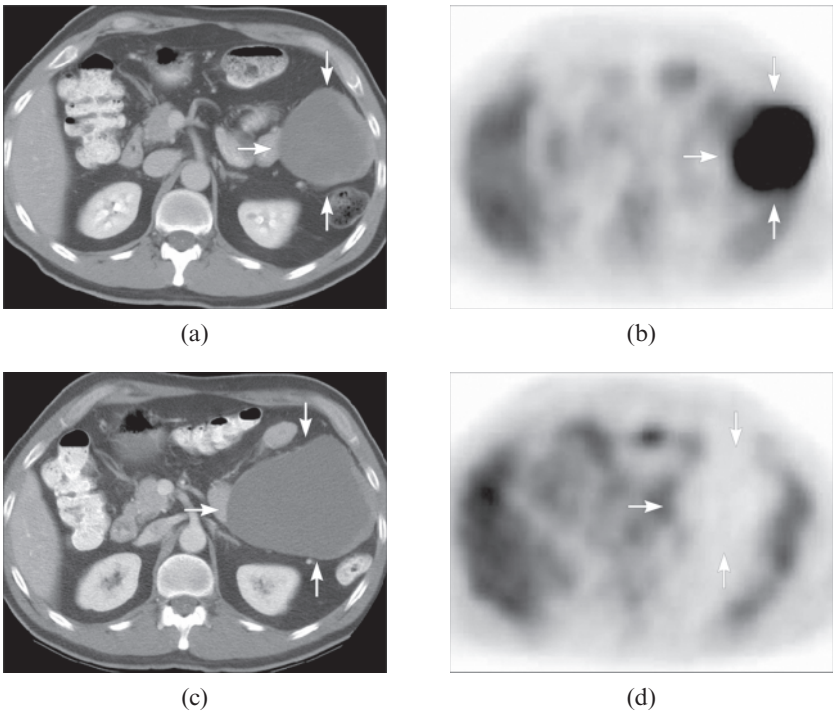

Figure 1. A patient with a primary gastrointestinal stromal tumour in the colon. The pre-treatment CT scan (a) shows a peritoneal mass (arrows), corresponding to a lesion with markedly increased fludeoxyglucose (FDG) uptake on the positron emission tomography (PET) scan (b). The CT scan (c) obtained 2 months after treatment showed that the mass had become larger; however, there was no appreciable FDG uptake seen on the FDG PET scan (d), which corresponded to clinical improvement. Reproduced with permission from Choi et al [7].

^{13}C-labelled cell metabolites can be used to detect early evidence of treatment response. The intention is not to provide an encyclopaedic review of the substrates that have been hyperpolarised and how they have been used, since there are many recent reviews that have covered this area [8–13], but rather to critically evaluate these hyperpolarised methods for detecting treatment response in comparison with existing radionuclide and MRI methods, with a particular focus on the work of my laboratory.

Metabolic imaging with hyperpolarised ^{13}C-labelled cell metabolites

Imaging tissue water protons, which are present in tissues at concentrations of ~80 M, can be used to produce relatively high-resolution three-dimensional images of tissue anatomy (in pre-clinical studies at high magnetic fields, isotropic image resolutions of ~10 μm are possible [14]). We have also known since the 1970s that it is possible to detect MR signals from tissue metabolites [15]. The problem is that these are present at ~10 000 times lower concentration than tissue water protons and therefore it is not possible to image them at clinical magnetic field strengths, except at relatively low spatial (1 cm^3) and temporal (5–10 min) resolution [16]. Moreover, single spectra or spectroscopic images of tissue metabolites lack dynamic information about metabolic fluxes. The lack of sensitivity has inhibited application of MR spectroscopy in the clinic, so that while in some centres spectroscopy is used routinely, particularly ^{1}H spectroscopy [16–18], it is not used both widely and routinely. Hyperpolarisation of ^{13}C-labelled cell substrates increases their sensitivity to detection in the MR experiment by more than 10 000-fold, making it possible to image not only the location of a hyperpolarised ^{13}C-labelled cell substrate in the body but also, more importantly, the kinetics of its conversion into other cell metabolites, with spatial resolutions of 2–5 mm and temporal resolutions in the subsecond range [19]. The technique promises unprecedented insights into tissue metabolism *in vivo*, which could have important clinical applications.

Physical principles

The MR experiment is insensitive because it depends on a weak interaction between a nuclear spin and a magnetic field. For a spin one-half nucleus, such as ^{1}H or ^{13}C, the populations of the two allowed energy levels are given by the Boltzmann distribution:

$$N_{\text{upper}} \Big/ N_{\text{lower}} = e^{\frac{-\Delta E}{kT}} \quad (1)$$

where ΔE is the energy difference between the spin states, k is the Boltzmann constant and T is the temperature in Kelvin. The conventional approach to increasing sensitivity has been to increase the magnetic field strength [*i.e.* increase the ΔE term in Equation (1)]. However, lowering the temperature can also increase polarisation. The problem is that to substantially increase the nuclear spin polarisation the temperature must be taken to almost absolute zero, which is difficult to do. The solution to this problem, which was first suggested theoretically by Albert Overhauser in 1953 [20], is to transfer polarisation from an electron spin to a nuclear spin. The nuclear spins are mixed with electron spins (on a stable radical), rapidly frozen to form a glass and placed in a magnetic field. For some substrates a glassing agent, such as glycerol, must be used. At ~1 K, which can readily be achieved by boiling off helium under vacuum (at ~100 Pa), the electron spins become completely polarised. The electron spin polarisation can then

be transferred to the nuclear spins by irradiating the electron spin resonance, which is in the microwave range (GHz). The key development, which has made possible the metabolic imaging experiments described here, was the realisation by Klaes Golman, Jan Henrik Ardenkjaer-Larsen and their colleagues that the polarised nuclear spins can be warmed rapidly to room temperature with substantial retention of the polarisation that was present in the frozen solid state [21]. This is achieved by rapidly dissolving the frozen sample in pressurised superheated water at ~180 °C. The gain in sensitivity for the solution state experiment is dramatic (Figure 2). The major problem with the technique is that the polarisation is relatively short lived, typically 10–30 s for hyperpolarised ^{13}C-labelled compounds *in vivo*, which means that injection and migration of the labelled compound to the target tissue and subsequent imaging must be accomplished within a few minutes. This also means that for any hyperpolarised ^{13}C-labelled cell substrate to be useful the cell must take it up and metabolise it very rapidly. The polarisation lifetime can be maximised by minimising ^{13}C–^{1}H intramolecular dipolar relaxation; this has usually been accomplished by placing the ^{13}C label in a carboxyl or carbonyl group, although replacement of protons with deuterons has also met with some success and could widen the range of usable substrates [22, 23]. In principle, any nucleus can be polarised, although attention has been focused largely on ^{13}C-labelled compounds because of their relatively long T_1s (long polarisation lifetime) and the ready commercial availability of ^{13}C-labelled cell metabolites that could be used to probe tissue metabolism. The inevitable dilution that accompanies the dissolution process requires that the ^{13}C-labelled cell substrate is polarised at high concentration, which imposes a further limitation in that these substrates must be very soluble in water. Nevertheless, despite these limitations, there are now numerous examples of hyperpolarised ^{13}C-labelled cell substrates whose metabolism has been detected *in vivo*, including [1-^{13}C]pyruvate, [1-^{13}C]lactate, [1,4-^{13}C$_2$]fumarate,

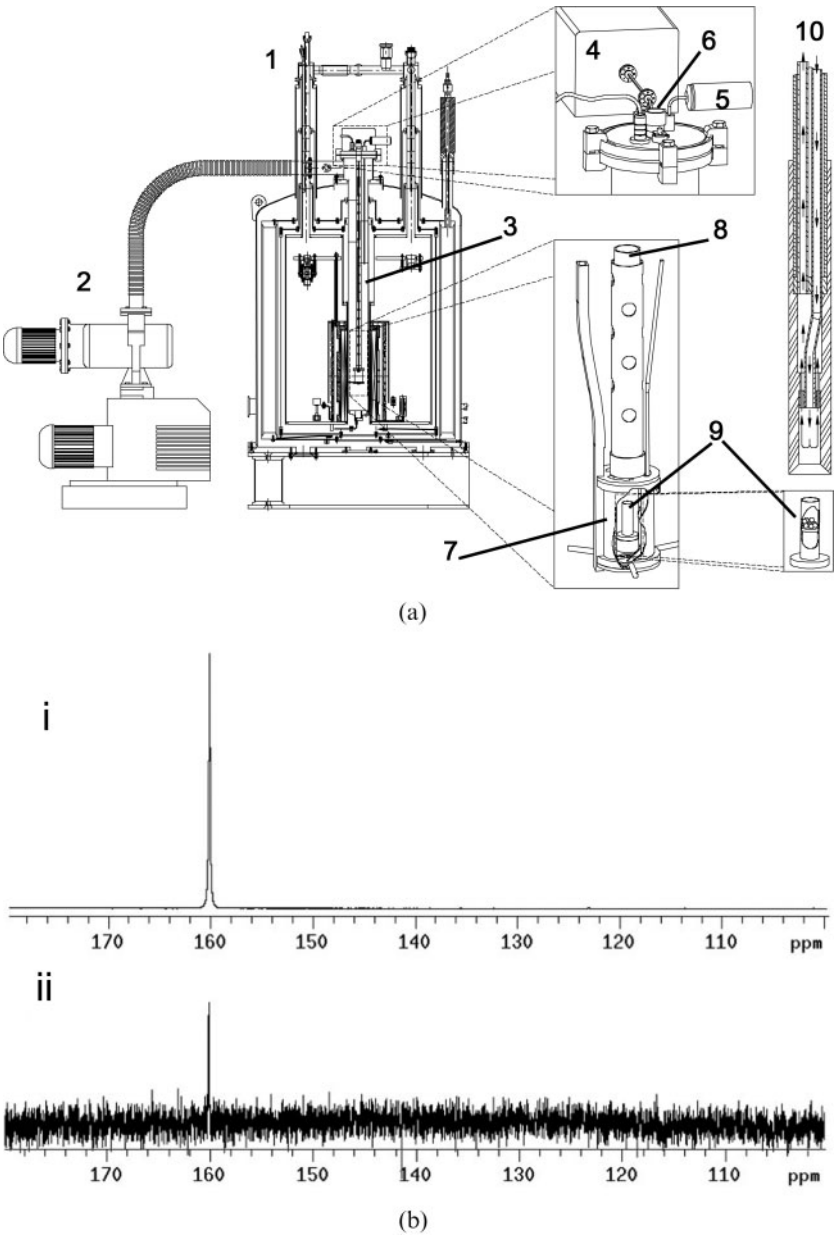

Figure 2. (a) The dynamic nuclear polarisation polariser and parts. 1, polariser magnet (operating at 3.35 T); 2, vacuum pump; 3, variable temperature insert (VTI); 4, microwave source; 5, pressure transducer; 6, sample port; 7, microwave cavity; 8, sample holder; 9, sample cup; 10, dissolution wand. A frozen sample to be polarised is placed in the sample cup (9) and the sample holder (8) is lowered into the VTI (3). Liquid helium from the magnet cryostat (1) is bled onto the sample using a needle valve. The sample temperature is lowered to ~1 K by applying a vacuum and is irradiated via the microwave cavity (7) using a microwave source (4) operating at 94 GHz. When the sample is fully polarised, which can be determined by monitoring the solid-state signal (a ^{13}C tuned coil is built into the sample holder), the sample undergoes the dissolution process. After releasing the vacuum the dissolution wand (10) is inserted into the sample holder in the VTI (3), where it engages with the sample cup (9). The sample is then lifted out of the liquid helium and discharged from the sample cup using superheated water at ~1000 kPa (see flow arrows in 10). (b) (i) ^{13}C spectrum of hyperpolarised urea (natural abundance ^{13}C). The concentration of urea was 59.6 mM and the polarisation was 20%. (ii) Thermal equilibrium spectrum of the same sample at 9.4 T and room temperature. This spectrum was acquired under Ernst-angle conditions (pulse angle of 13.5° and repetition time of 1 s based on a T_1 of 60 s) with ^{1}H decoupling. The spectrum is the sum of 232 128 transients collected over 65 h. Reproduced with permission from Ardenkjaer-Larsen et al [21].

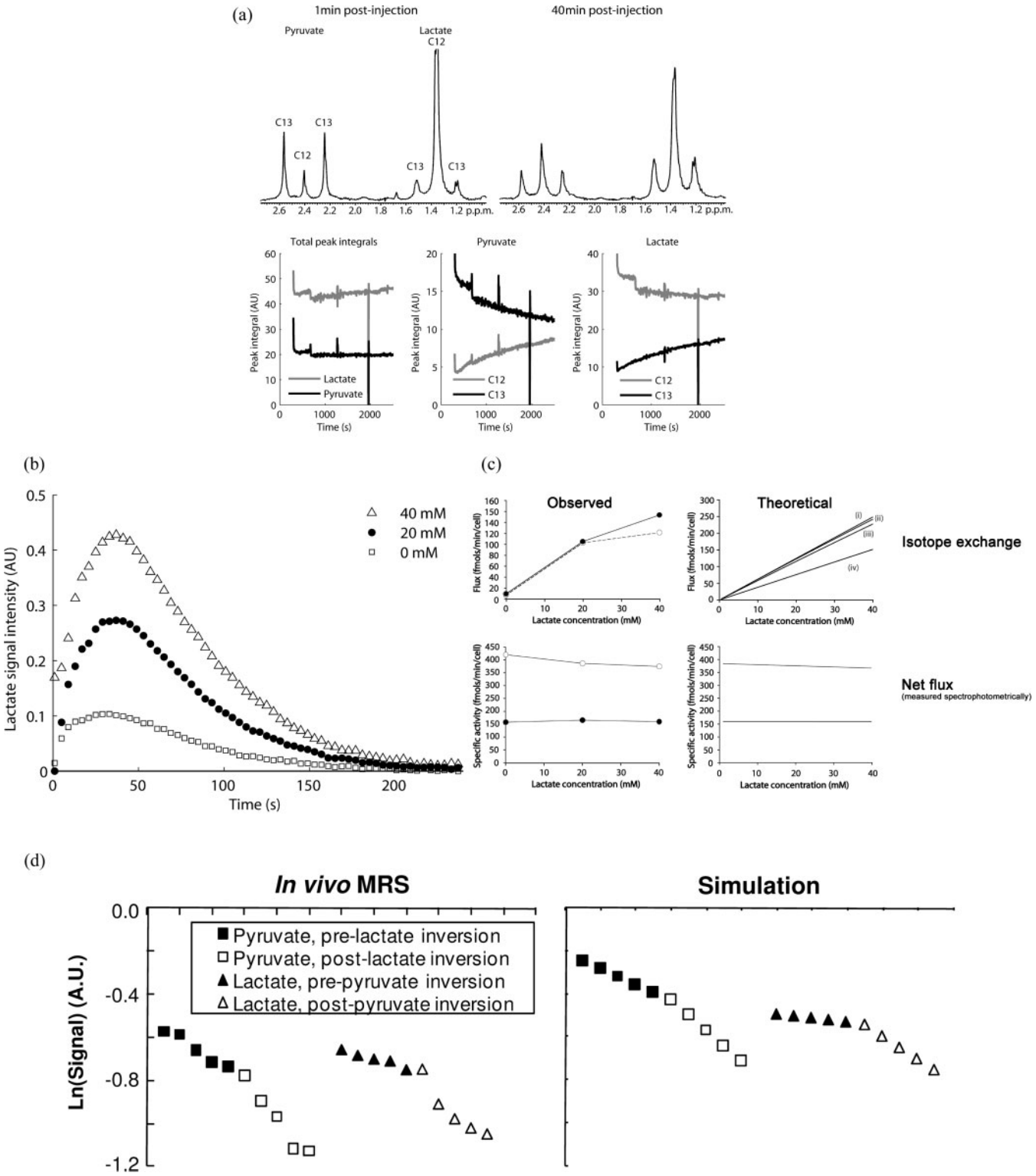

Figure 3. Hyperpolarised [1-^{13}C]pyruvate exchanges the ^{13}C label with lactate in tumour cells *in vitro* and in tumours *in vivo*. (a) Addition of non-hyperpolarised [3-^{13}C]pyruvate to a tumour cell suspension containing added lactate, in which the ^{13}C label was detected indirectly in the proton spectrum, demonstrated that there was exchange of label between lactate and pyruvate. The ^{1}H spectrum allows the concentrations of both the ^{13}C-labelled and unlabelled species to be observed and shows that there is a decrease in the concentration of ^{13}C-labelled pyruvate and a corresponding increase in the unlabelled form (^{12}C). (b) Addition of lactate to a tumour cell suspension together with hyperpolarised [1-^{13}C]pyruvate increases the rate of label flux between pyruvate and lactate. This is not what you would expect if there was net flux (see c), where addition of lactate inhibits flux between pyruvate and lactate, but is what you would expect to see if there is exchange of isotope between pyruvate and lactate. The filled symbols in (c) represent experiments with 20 mM pyruvate and the open circles with 2 mM pyruvate. These experiments also demonstrate that there is pyruvate inhibition of the enzyme in spectrophotometric measurements of net flux but not in the MR spectroscopic (MRS) measurements of hyperpolarised ^{13}C label exchange. The lack of pyruvate inhibition in the latter experiments can be explained by the higher enzyme concentration (see Witney et al [29]). (d) Exchange of

hyperpolarised ^{13}C label between endogenous lactate and the injected [1-^{13}C]pyruvate can also be demonstrated using magnetisation transfer measurements *in vivo*. Inversion of the lactate polarisation produces an increase in the rate of decrease of the pyruvate signal, demonstrating unequivocally that there is label exchange, with hyperpolarised label being transferred back to pyruvate from lactate. AU, arbitrary unit. Reproduced with permission from Day et al [24], Witney et al [29] and Kettunen et al [32].

^{13}C-bicarbonate, [2-^{13}C]fructose, [1-^{13}C]ketoisocaproate, [5-^{13}C]glutamine and [1-^{13}C]glutamate [13].

Detecting treatment response with hyperpolarised [1-^{13}C]pyruvate

Since [1-^{13}C]pyruvate has been the most widely used hyperpolarised substrate to date, including for tumour response monitoring [24, 25], and was the first to be used in a clinical trial of the technique [12], it is perhaps worth considering what information it provides about tumour metabolism *in vivo*. Hyperpolarised [1-^{13}C]pyruvate exchanges label with endogenous lactate and alanine, in the reactions catalysed by lactate dehydrogenase (LDH) and alanine aminotransferase, respectively. $^{13}CO_2$ can also be produced in the irreversible oxidative decarboxylation reaction catalysed by mitochondrial pyruvate dehydrogenase in those tissues with high levels of mitochondrial metabolism, such as the heart [26, 27]. Only very low or undetectable levels of $^{13}CO_2$ and $H^{13}CO_3^-$, with which $^{13}CO_2$ is in rapid exchange, have been observed in tumours. The experimental evidence that pyruvate exchanges hyperpolarised ^{13}C label with endogenous unlabelled lactate is summarised in Figure 3. The reaction catalysed by LDH is near to equilibrium in the cell and the equilibrium constant is such that when pyruvate enters the cell the reaction will rapidly re-establish chemical equilibrium, with only a very small net conversion of pyruvate into lactate [13, 24]. What is then observed in the ^{13}C MR measurements is predominantly the slower isotopic equilibration of hyperpolarised ^{13}C label between the injected pyruvate and the endogenous lactate pool. Thus, hyperpolarised lactate will generally be observed in those tissues that have a large endogenous lactate pool, such as tumours. This explains why the reverse experiment with hyperpolarised [1-^{13}C]lactate has not been so successful [28] since endogenous pyruvate is present at much lower concentrations than lactate.

In a tumour, the observed rate of hyperpolarised ^{13}C label exchange will depend on the rate of pyruvate delivery to the tumour, the rate of pyruvate transport into the cell and the activity of LDH. The relative importance of transport rate and LDH activity on the kinetics of the observed exchange has recently been considered, both experimentally and theoretically [29]. This showed that control of the exchange is shared between the transporter and LDH and that this varies according to the lactate and pyruvate concentrations. The observed exchange kinetics for LDH were well described by an ordered ternary complex mechanism, in which the coenzymes nicotinamide adenine dinucleotide (NAD^+) and NADH (the reduced form of NAD^+) bind first [Equation (2)], and by using rate constants that had been determined previously for the rabbit muscle enzyme using steady-state kinetic studies. This analysis showed that the apparent K_m of LDH for pyruvate is 13 μM, where K_m is the Michaelis constant, defined as the substrate concentration at which the enzyme shows half the maximal velocity. The analysis also showed that there is little pyruvate inhibition of the enzyme at the enzyme concentrations found in the cell and that the exchange rate is linearly dependent on the endogenous lactate concentration. The observed K_m for pyruvate in cells is higher, depending on the extent to which the transporter limits the exchange [29, 30].

In many studies, with both tumour cells *in vitro* and tumours *in vivo*, the rate constant describing exchange of hyperpolarised ^{13}C label between pyruvate and lactate (k_P) has been determined by fitting the pyruvate and lactate peak intensities to the modified Bloch equations for two site exchange [24] [Equations (3)–(5)].

$$E + \mathrm{NAD}^+ \Leftrightarrow E.\mathrm{NAD}^+ + \mathrm{Lactate} \Leftrightarrow E.\mathrm{NAD}^+.\mathrm{Lactate} \Leftrightarrow E.\mathrm{NADH.Pyruvate} \Leftrightarrow E.\mathrm{NADH} + \mathrm{Pyruvate} \Leftrightarrow E + \mathrm{NADH} \quad (2)$$

$$\mathrm{L} \underset{k_P}{\overset{k_L}{\rightleftharpoons}} \mathrm{P} \quad (3)$$

$$dLz/dt = -\rho_L(Lz - L\infty) + k_P Pz - k_L Lz \quad (4)$$

$$dPz/dt = -\rho_P(Pz - P\infty) + k_L Lz - k_P Pz \quad (5)$$

L_z and P_z are the z magnetisations of the ^{13}C nucleus in the lactate and pyruvate carboxyl carbons, ρ_L and ρ_P are the spin lattice relaxation rates and L_∞ and P_∞ are the equilibrium magnetisations (*i.e.* at $t=\infty$). In some studies an arterial input function has also been included [31]. This simple analysis provides a robust estimate of k_P that is relatively insensitive to the values of ρ_L or ρ_P, or to assumptions that may be made about their values in order to facilitate data fitting; for example, that $\rho_L=\rho_P$ [32]. The data can often be fitted by setting k_L to zero, with little effect on the estimated value for k_P. However, this does not mean that there is no exchange (see above), only that the value for k_L is poorly determined by an experiment with [1-^{13}C]pyruvate. In many studies only a value for the first order rate constant, k_P, has been reported rather than the biochemically relevant flux (in $mM\,s^{-1}$) since the latter requires an estimate of the pyruvate concentration in the image voxel. In the future considerable effort will be required to derive robust estimates of concentration and thus flux, particularly in a clinical setting.

Clearly any drug that affects the concentration of LDH or its substrates, or affects the levels of the monocarboxylate transporters (MCTs), which transport pyruvate and lactate across the cell plasma membrane, or affects pyruvate delivery to the tumour [33] will have an effect on the kinetics of lactate labelling by hyperpolarised [1-^{13}C]pyruvate. The first study on response monitoring

with hyperpolarised [1-^{13}C]pyruvate was in a murine lymphoma model, which showed that there was decreased lactate labelling within 24 h of treatment with the chemotherapeutic drug etoposide [24]. In cells this was shown to be due to a deoxyribonucleic acid (DNA) damage response, which led to activation of poly-adenosine diphosphate ribose polymerase (PARP) and consequent depletion of the NAD^+ pool; NAD^+ is a substrate for PARP. Addition of a PARP inhibitor preserved the NAD(H) pool and delayed the loss of label exchange between pyruvate and lactate. In tumours, the loss of exchange post-etoposide treatment was shown to be due to a number of factors, including loss of NAD(H) and decreases in tumour lactate and LDH concentrations. A small molecule MCT inhibitor has been shown to inhibit the exchange [30], as have drugs that modulate LDH concentration through inhibition of the phosphatidylinositol 3-kinases (PI3K)-protein kinase B (PKB) (Akt) pathway [25, 29]. The hyperpolarised [1-^{13}C]pyruvate experiment thus offers a novel way of monitoring PI3K–Akt pathway inhibition non-invasively *in vivo*, which has become an important drug target [34]. Since the central pathways of metabolism are so highly interconnected, in a so-called ''scale-free'' network, where perturbation of any part of the network is communicated as metabolite changes throughout the network [35], it is likely that the hyperpolarised [1-^{13}C]pyruvate experiment will be exquisitely sensitive to the effects of many different drugs.

Monitoring treatment response with hyperpolarised [1-^{13}C]pyruvate is analogous to monitoring treatment response with FDG PET, and the two methods have been compared directly [36]. In a murine lymphoma model the FDG PET experiment gave an earlier indication of treatment response than the pyruvate experiment, which was shown to be due to an early downregulation of the glucose transporters (GLUTs) 1 and 3 at the plasma membrane. However, although FDG PET gave an earlier indication of response, the amplitude of the changes in FDG uptake and lactate labelling were comparable, suggesting that the two techniques would have similar sensitivities for detecting treatment response in the clinic. If this were the case then what would be the advantage(s) of using the polarised pyruvate experiment? The FDG PET experiment does not work well in some tumour types; the prostate shows relatively low levels of FDG uptake, and high levels in the adjacent bladder make quantification of the signal more difficult and in the brain high levels of FDG uptake in normal surrounding brain tissue can mask tumour uptake. Both are tumour types in which the hyperpolarised pyruvate experiment has been shown to work well [37–39]. In a study of response to radiotherapy in a rat brain model of glioma, lactate labelling was shown to decrease following treatment, despite a continued increase in tumour size observed in contrast agent-enhanced MR images (Figure 4) [39]. An important advantage of the FDG PET experiment is that it is a whole body imaging technique and thus can be used to monitor several tumours simultaneously (*e.g.* the primary tumour and its metastases).

Detecting cell death with hyperpolarised [1,4-^{13}C]fumarate

Polarised pyruvate MR spectroscopy and FDG PET measurements can show whether a tumour is responding to treatment, and thus whether a drug has hit its target, but not necessarily whether the treatment has killed any tumour cells. A decrease in lactate labelling or FDG uptake might indicate a loss of cells within the tumour, but equally well could reflect some metabolic change; for example, a decrease in LDH activity through changes in its substrate concentrations or downregulation of the GLUTs at the plasma membrane. Because cell death soon after treatment can be a good prognostic indicator for treatment outcome, considerable effort has gone into the development of imaging methods that detect cell death more specifically. These include agents that bind the phospholipid phosphatidylserine (PS), which is exposed by dying cells [4], ^{18}F-labelled molecules that bind to activated caspase-3/7 [40], which is increased in apoptotic cells, and diffusion-weighted MRI, which detects a loss of tumour cellularity through an increase in the apparent diffusion coefficient of tissue

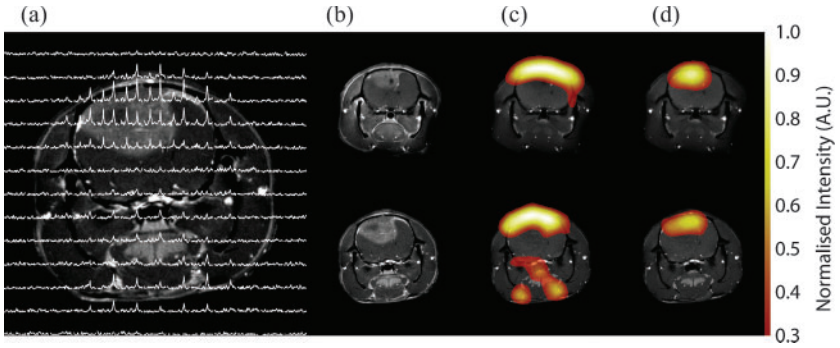

Figure 4. Imaging response to radiotherapy in a rat brain glioma model. A ^{13}C chemical shift spectroscopic image obtained following the intravenous injection of hyperpolarised [1-^{13}C]pyruvate is shown in (a), superimposed on a ^{1}H image of tissue anatomy. The chemical shift images were obtained from a 6-mm axial slice with an in-plane resolution of $2.53 \times 2.53\,mm^2$. The tumour, which is readily observed in the contrast agent-enhanced image (b), was observed to increase in size following radiotherapy (lower image). However, the corresponding ^{13}C images of pyruvate (c) and lactate (d), which were derived from spectroscopic images similar to those shown in (a), clearly show a relative decrease in lactate signal post therapy [compare signal intensities in the upper (before treatment) and lower images (after treatment)]. AU, arbitrary unit. Reproduced with permission from Day et al [39].

water [41]. The fundamental problem with the targeted agents that bind PS or activated caspase is non-specific background binding, which is a problem for any targeted molecular imaging agent. The difficulty is not to get the targeted agent to bind its specific target but rather to minimise the non-specific background binding, which will limit the generation of image contrast. This problem is illustrated by our experience with a PS-targeted agent based on the C2A domain of the protein synaptotagmin. The protein has been labelled with superparamagnetic iron oxide nanoparticles and with Gd^{3+} chelates and has been shown to detect dead or dying tumour cells *in vivo* in T_2 and T_1 weighted images, respectively [42, 43], as illustrated for the Gd^{3+} chelate-labelled agent in Figure 5. Although the accumulation of the agent in the tumour at 24 h after drug treatment is clear in these false colour images, the concentration of the agent in treated tumours was only twice that in the untreated controls. By labelling the agent with both Gd^{3+} chelates and with a fluorophore we were able to show by fluorescence microscopy measurements on tumour sections obtained following the MRI measurements that the MR agent was indeed binding to dead cells in the tumour. Fluorescence from labelled C2A was co-localised with a terminal deoxynucleotidyl transferase dUTP nick end labelling (TUNEL) stain, which detects DNA damage in dead cells (Figure 5). However, it is also evident from these fluorescence images that there was a low level of non-specific background binding, in which C2A was apparently bound to viable cells. In these high-resolution microscopy images this background is not a problem and the increased binding of C2A to the regions of dead, TUNEL-positive, cells is clearly evident. In a lower resolution image however, such as an MR image, the background binding will add up and reduce the contrast-to-background ratio. Analysing regions of interest, which is what is done routinely in analysing data of this sort, exacerbates the problem by effectively further reducing the resolution of the MR image and discarding important information on contrast agent distribution. We recaptured this information, and thus improved the sensitivity of cell death detection, by parameterising the distribution of C2A in a treated tumour using an image analysis technique that had been used previously by the astrophysics community to analyse images of galaxies [44]. The distribution of C2A in a treated tumour was much more heterogeneous than in an untreated tumour, reflecting the heterogeneous distribution of cell death that was evident in the microscopy images (Figure 5). By quantifying this heterogeneity we were able to substantially improve the sensitivity of detection of cell death.

Despite being able to improve C2A detection of dead cells by analysing its distribution, non-specific background binding remains a significant problem. This general problem in molecular imaging has been addressed previously by using ''molecular beacons''—molecules that generate a signal *de novo*, in the absence or with low levels of background signal. Well-known examples include firefly luciferase, which generates light in the presence of luciferin, oxygen and adenosine triphosphate [45], and protease-sensitive fluorescence agents, in which cleavage of a peptide bond within the

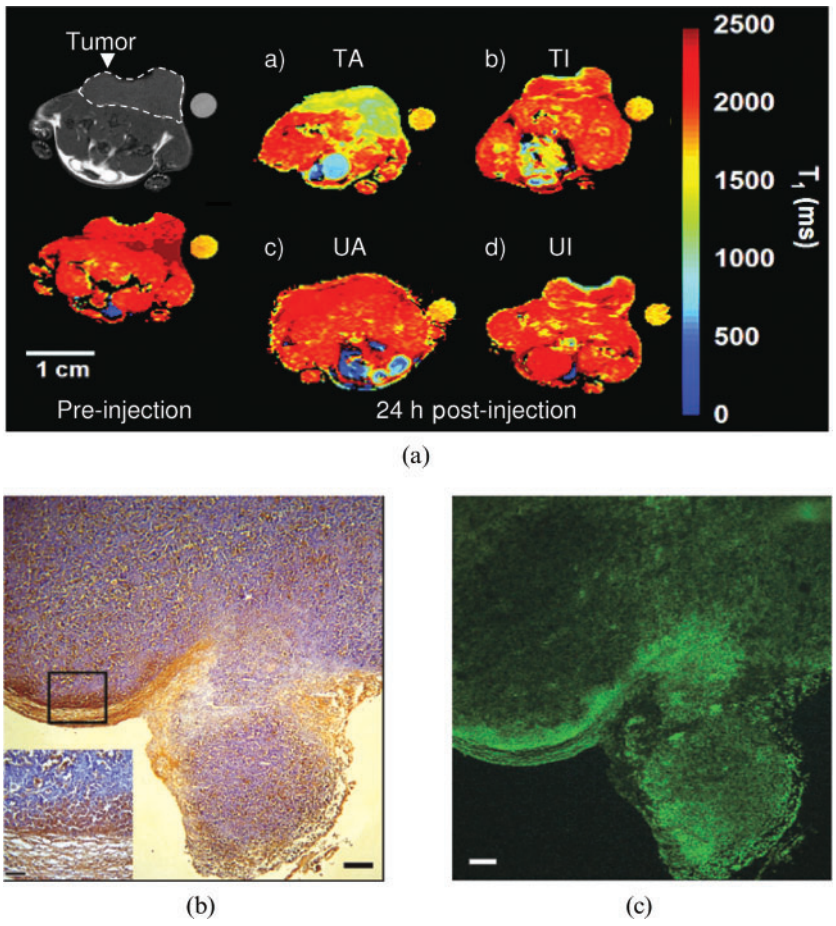

Figure 5. Non-specific binding limits the contrast that can be achieved using a targeted MR contrast agent. (a) Injection of a Gd^{3+} chelate-conjugated agent that binds to dead cells showed significant accumulation in a treated tumour at 24 h after injection (TA) (a), whereas a site-directed mutant of the protein, which was inactive, showed less accumulation (TI) (b). Neither the active nor inactive agent showed accumulation in the untreated tumours (UA and UI) (c, d). Co-labelling of the active agent with a fluorescent probe showed that it was bound to dying cells. (c) A fluorescence image of a histological section obtained from a treated tumour following the MRI experiment. Regions where the probe is bound, which are yellow in (c), were co-localised with regions of cell death, which are stained brown (terminal deoxynucleotidyl transferase dUTP nick end labelling stain) in (b). While the agent clearly binds to areas of cell death, it also appears to show non-specific binding to regions of viable cells and it is this that reduces the contrast-to-background ratio in the lower resolution MR images.

agent leads to generation of fluorescence [46]. Detection of cell death in the absence of a background signal has been achieved using the hyperpolarised substrate, [1,4-^{13}C]fumarate [47]. In viable cells there is no detectable uptake of hyperpolarised [1,4-^{13}C]fumarate within the relatively short lifetime of the polarisation. However, in dying or necrotic cells, where the plasma membrane permeability barrier has been compromised, there is rapid uptake of labelled fumarate and subsequent hydration, in the reaction catalysed by the enzyme fumarase, to form hyperpolarised [1,4-^{13}C]malate. We have demonstrated in tumour cells *in vitro* and tumours *in vivo* a linear correlation between the levels of cell necrosis and the rate of malate formation [33, 47, 48]. Given that fumarase is ubiquitous in biological systems and the only other substrate required is water, this could be a general method for detecting cell death *in vivo*. It has the advantage over other methods of detecting cell death in that there is no background. If labelled malate is observed then current evidence suggests that there must be dead cells present within the image voxel. The technique has already been demonstrated in different tumour types and with different types of drugs, including antivascular drugs, such as combretastatin A4 phosphate, in which we showed that measurements of hyperpolarised pyruvate and fumarate metabolism could provide a more sustained and sensitive indicator of response to this vascular disrupting agent than dynamic contrast agent-enhanced or diffusion-weighted MRI, respectively [33]. There is also evidence that this technique could be used to detect necrosis in other tissues [49], including the kidney [50]. Potential disadvantages of using hyperpolarised [1,4-^{13}C]fumarate to detect cell death include possibly low levels of fumarase in some tumour types and washout of the enzyme from the necrotic cell, which would limit the time period over which necrosis could be detected. The latter may, however, also be an advantage in the context of detecting early tumour responses to treatment in that only recently killed cells should be detected.

Hyperpolarised ^{13}C-labelled glutamine and glutamate

Another hyperpolarised substrate that could be valuable in detecting tumour treatment response is [5-^{13}C]glutamine. It has long been known that tumours show upregulated glutamine utilisation, the amino acid being used for the generation of metabolic intermediates involved in macromolecular biosynthesis, which supports the increased growth rate of tumour cells, and also the synthesis of glutathione, which is an important cellular anti-oxidant [51]. The rapid growth rate of tumours leads to increased production of reactive oxygen species (ROS) and it is becoming increasingly clear that the metabolism of tumours is adapted to cope with this oxidative load by upregulation of anti-oxidant systems, such as increased glutathione production and pentose phosphate pathway activity [51]. The cellular oncogene *MYC*, which encodes a transcription factor that promotes cell proliferation, is directly involved in glutamine utilisation, upregulating the expression of the glutamine transporters and of a glutaminase isoform, in the latter case by repressing the expression of a micro-ribonucleic acid [52]. We have shown that the glutaminase activity in human hepatoma cells can be measured by monitoring the conversion of hyperpolarised [5-^{13}C]glutamine into glutamate [53]. The problem with this substrate was that the polarisation lifetime of the label in the C-5 position was relatively short, ~16 s, which precluded its use *in vivo*. However, a recent study has shown that deuteration of the molecule (to produce L-[5-^{13}C-4-2H_2]glutamine) results in a significant extension of the polarisation life time [23], raising the possibility that this substrate could be used to monitor tumour glutaminase activity *in vivo*. Here it might be used as a surrogate for Myc expression and to assess inhibition of tumour cell proliferation, in much the same way as 3′-deoxy-3′-[^{18}F]fluorothymidine uptake has been used as a cell proliferation marker in PET [54, 55].

Mammalian cells express >60 dioxygenases that utilise α-ketoglutarate (α-KG), an intermediate in the tricarboxylic acid cycle, as a co-substrate, including the prolyl hydroxylases that control the stability of hypoxia-inducible factor (HIF1), and the histone demethylases and the ten–eleven translocation family of 5-methylcytosine hydroxylases. Many of these α-KG-dependent dioxygenases have a K_m for α-KG near physiological concentrations, suggesting that its concentration may influence HIF1 stability and gene expression [56, 57]. We have shown recently, using hyperpolarised [1-^{13}C]glutamate, that we can detect, for the first time, α-KG in a tumour *in vivo* [58], raising the possibility that we may be able to interrogate the potential role of α-KG in controlling gene expression and HIF1 stability in a tumour.

Monitoring the tumour microenvironment: pH and redox state

The tumour microenvironment can have a profound influence on tumour aggressiveness, treatment response and metastatic spread. We have demonstrated that tumour extracellular pH can be imaged from the ratio of the signal intensities of hyperpolarised $H^{13}CO_3^-$ and $^{13}CO_2$ following intravenous injection of hyperpolarised $H^{13}CO_3^-$ [59] and, more recently, that the tumour redox state can be determined by monitoring the oxidation and reduction of hyperpolarised [1-^{13}C]ascorbate and [1-^{13}C]dehydroascorbate, the reduced and oxidised forms of vitamin C, respectively [60] (Figure 6). The polarised bicarbonate experiment showed, as expected, that the tumour extracellular space has a low pH, as has been observed using other MR probes in pre-clinical animal models [61]. Similarly, the hyperpolarised ascorbate experiment demonstrated, as has become apparent from recent work, that tumours maintain a highly reduced microenvironment [51]. In tumour cell suspensions, in which there is production of ROS, there was observable oxidation of [1-^{13}C]ascorbate. However, when these same cells were implanted to form subcutaneous tumours and the [1-^{13}C]ascorbate was injected intravenously there was no detectable oxidation in the tumours. When [1-^{13}C]dehydroascorbate was injected into these animals, which is rapidly transported into tumour cells on GLUT1, then very rapid reduction to ascorbate was observed. This would explain why we failed to see ascorbate oxidation since any dehydroascorbate will

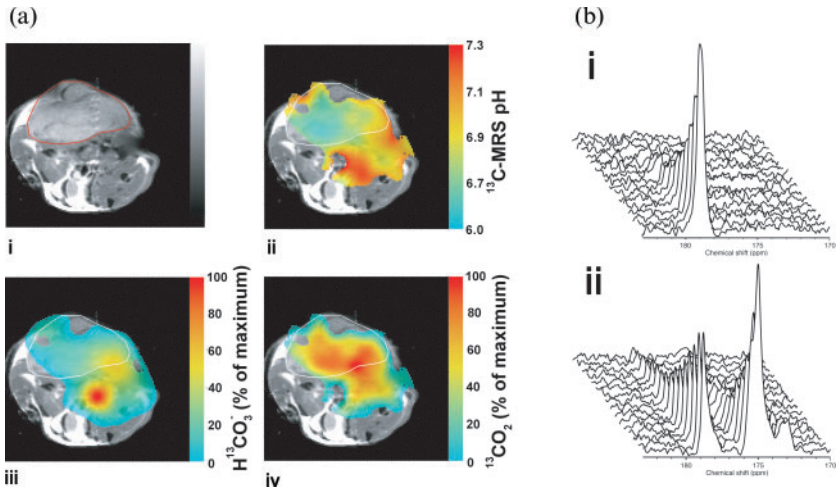

Figure 6. Monitoring the tumour microenvironment. (a) The false colour images in (iii) and (iv) show the distribution of labelled HCO_3 and CO_2 following intravenous injection of hyperpolarised ^{13}C-labelled HCO_3^- into a tumour-bearing mouse. The image resolution was 16×16 voxels, each of which measured 2×2×6 mm. The images were smoothed by multiplying by a cosine function and zero filling to 128 points in both spatial directions, line broadening to 30 Hz and then zero filling to 512 points in the spectral direction before Fourier transformation. HCO_3^- and CO_2 peaks were fitted in the frequency domain and only pixels with a frequency separation between the two peaks of 36 ± 1 ppm were included. These ^{13}C spectroscopic images are superimposed on a ^{1}H image of tissue anatomy (i). The tumour margin is outlined in red in (i) and in white in (ii–iv). The ratio of the CO_2 (iv) and HCO_3^- (iii) images can be used to calculate an image of extracellular pH (ii). (b) ^{13}C MR spectra acquired from tumours following intravenous injection of [1-^{13}C]-ascorbic acid (i) and [1-^{13}C]-dehydroascorbic acid (ii). Sequential spectra were collected over a period of 16 s (i) and 32 s (ii). While there was no observable flux of hyperpolarised ^{13}C label from [1-^{13}C]-ascorbic acid (179 ppm) to [1-^{13}C]-dehydroascorbic acid (175 ppm) (i), significant label flux was observed from [1-^{13}C]-dehydroascorbic acid to [1-^{13}C]-ascorbic acid, indicating rapid reduction of the injected [1-^{13}C]-dehydroascorbic acid in the tumour. Reproduced with permission from Gallagher et al [59] and Bohndiek et al [60].

be rapidly taken up and re-reduced and is entirely consistent with the current view that tumours have upregulated anti-oxidant systems to cope with the increased ROS load.

Prospects for clinical translation

The hyperpolarised ^{13}C MR experiment has already taken its first steps to clinical translation with a trial of hyperpolarised [1-^{13}C]pyruvate in prostate cancer, which commenced at the University of California at San Francisco, CA, in November 2010 and where the aim was to use it to detect treatment response (ClinicalTrials.gov identifier: NCT01229618). A 250 mM pyruvate solution was injected at up to 0.43 ml kg^{-1}, which equates to a blood concentration of ~1.5 mM, and spectroscopic images were acquired using a custom-designed ^{13}C transmit volume coil and a ^{1}H/^{13}C endorectal receive coil in conjunction with a 3 T whole body scanner. Such a coil arrangement is also likely to be used for superficial tumours in other abdominal regions such as the breast and lymph nodes. Despite the enormous gain in sensitivity obtained through hyperpolarisation, its transient nature, which precludes signal averaging, means that detectable signal is still limited and places a premium on getting the receiver coil as close as possible to the target tissue. Although such hardware is currently not widely available in hospital radiology departments, the coils are relatively inexpensive and the experiments could reasonably be implemented on any modern scanner with spectroscopy capability. This first trial employed an adapted pre-clinical polariser, which had to be used in a clean room and which would not be appropriate for routine clinical use. However, a hyperpolariser intended for clinical use has been described recently [62].

The relatively short lifetime of the polarisation and the dynamic nature of the metabolic labelling that results from injection of a hyperpolarised ^{13}C-labelled molecule has necessitated the development of very fast MR spectroscopic imaging techniques that make efficient use of the short-lived polarisation (reviewed recently in [13]). Much of the information in these experiments is in the kinetics of metabolite labelling and therefore ideally one should collect multiple images over the lifetime of the polarisation (2–3 min), in which fitting of individual pixel intensities to a kinetic model can be used to produce metabolic rate maps. The majority of the pre-clinical studies have used pulse sequences based on gradient refocusing, such as echoplanar (spectroscopic) imaging [63, 64], spiral chemical shift imaging [65, 66] and rosette chemical shift imaging [67], which have produced nominal image resolutions of 5x5x10 mm^3 in under 1 s [19]. The likely spatial resolution in the clinic is open to debate but will probably be between 2 and 5 mm. In some instances, however, spatial resolution may not be that important. For example, when detecting cell death in a tumour with hyperpolarised [1,4-^{13}C]fumarate post treatment, acquisition of signal from the entire tumour volume may allow detection of diffuse cellular necrosis. A disadvantage of metabolic imaging with hyperpolarised ^{13}C, when compared with radionuclide imaging, is the relatively limited field of view that is imposed by the short lifetime of the polarisation. Thus, it is unlikely that hyperpolarised ^{13}C MR spectroscopic imaging will be able

to monitor simultaneously the metabolism of a primary tumour and its distant metastases.

Conclusion

In this review, I have taken a biochemical view of the field, reflecting my own interests and expertise. However, I believe that in the future radiology will move increasingly from a discipline that images tissue anatomy to one that images tissue function as well. Hyperpolarised ^{13}C MR spectroscopic imaging is a very promising tool for imaging tissue biochemistry, particularly in tumours, where it can be used to ask quite sophisticated questions about tumour biology and how this changes in response to treatment. If radiologists are to fully exploit the potential of this technique in the clinic then they will need to know more about the underlying biochemistry.

Metabolic imaging with hyperpolarised ^{13}C-labelled cell substrates has, with the first clinical trial of pyruvate in prostate cancer, taken its first steps on the road to clinical translation. Given that fumarate is used in some drug preparations and bicarbonate, glutamine and ascorbate have already been infused into patients at the concentrations needed for hyperpolarised MR studies, there is a reasonable expectation that these substrates will also translate to the clinic in the future. However, if this technique is to become widely used in radiology then we will need to find compelling applications: things which it can do much better than existing imaging technologies, which provide robust, readily interpretable and clinically meaningful results at a reasonable cost. Based on a growing body of pre-clinical data, it is perhaps reasonable to speculate now on what some of these might be. In the case of [1-^{13}C]pyruvate, which has been the most widely used hyperpolarised substrate to date, there are already some strong indications as to where it might be useful in oncology, for example for staging tumours [37] and monitoring early evidence of treatment response [24]. The important question with pyruvate is what advantages it might have over existing imaging techniques. In the case of treatment response monitoring, it would appear to have several advantages over the current gold standard in the clinic, FDG PET. In addition to being usable in those tumours where FDG PET does not work well, such as prostate and brain, it does not involve the use of ionising radiation. Although the radiation dose from FDG is low, current evidence suggests that the risk of excess cancer and heritable effects from PET/CT exposure is ~5% per sievert [68]; this may become an issue for repeat measurements, such as those that would be needed to guide treatment, and when examining children or females of childbearing age. With hyperpolarised ^{13}C-labelled substrates there are no obvious hazards associated with injecting molecules that are endogenous. Although injected at relatively high concentrations they clear quickly and thus it is possible to contemplate guiding treatment using these substrates in an image–treat–image–treat paradigm. Hyperpolarised bicarbonate might find use as a generic marker for detecting the presence of disease since almost all pathological states are accompanied by a low extracellular tissue pH, including tumours, ischaemia, infection, hypoxia and inflammation. However, the relatively short lifetime of the polarisation in this molecule might necessitate finding ways to inject the substrate closer to the site of disease. Since sites of inflammation are often hypoxic, they can also be detected using hyperpolarised [1-^{13}C]pyruvate [69]. Hypoxia can lead to increased lactate concentration and LDH activity, both of which will lead to proportional increases in the rate of lactate labelling [29]. In tumours a low extracellular pH has been correlated with tumour aggressiveness and metastatic potential and so hyperpolarised bicarbonate might also be used for staging tumours, as has been done with pyruvate. In the latter case increased lactate labelling was observed in the more aggressive tumours, presumably reflecting a higher endogenous lactate concentration [37]. Measuring the rate of dehydroascorbate reduction has never been possible before and, in the absence of information about what controls this rate, it is difficult to predict how it might be used clinically. However, since we have evidence that it is faster in tumours than in surrounding normal tissue it may be possible to use it to distinguish, for example, between benign and malignant lesions. It might also be used to detect the action of drugs targeted at the pathways responsible for maintaining the highly reduced state that seems to be a characteristic of tumours [51]. Hyperpolarised glutamine may have utility in detecting the activity of cytostatic drugs. However, since the aim of any tumour therapy is to kill tumour cells, then possibly the most promising agent for detecting treatment response is hyperpolarised [1,4-^{13}C]fumarate. Uniquely among the methods that my laboratory has used to detect cell death *in vivo* it seems to provide an unequivocal measure of cell death, which has no background signal.

It seems likely that the important clinical applications for hyperpolarised ^{13}C imaging will only be found through widespread utilisation of the technology at multiple research centres and could take some time, perhaps 10–15 years. However, the exciting developments in the pre-clinical arena, which have driven the rapid translation of the technique into the clinic, give reason to be optimistic that the technique will have an impact on the practice of radiology in the future.

Acknowledgments

The author acknowledges Cancer Research UK, the Leukemia and Lymphoma Society, the Wellcome Trust, the National Institute for Health Research Cambridge Biomedical Research Centre and GE Healthcare for support. I would also like to thank members of my laboratory, both past and present, for their efforts, insights and dedication that made much of the work described here possible.

References

1. Twombly R. Avastin's uncertain future in breast cancer treatment. J Natl Cancer Inst 103:458–60.
2. Sequist LV, Bell DW, Lynch TJ, Haber DA. Molecular predictors of response to epidermal growth factor receptor antagonists in non-small-cell lung cancer. J Clin Oncol 2007;25:587–95.
3. Sawyers CL. The cancer biomarker problem. Nature 2008;452:548–52.

4. Brindle K. New approaches for imaging tumour responses to treatment. Nat Rev Cancer 2008;8:94–107.
5. Eisenhauer E, Therasse P, Bogaerts J, Schwartz L, Sargent D, Ford R, et al. New response evaluation criteria in solid tumours: revised RECIST guideline (version 1.1). Eur J Cancer 2009;45:228–47.
6. Miller JC, Pien HH, Sahani D, Sorensen AG, Thrall JH. Imaging angiogenesis: applications and potential for drug development. J Natl Cancer Inst 2005;97:172–87.
7. Choi H, Charnsangavej C, Faria SD, Tamm EP, Benjamin RS, Johnson MM, et al. CT evaluation of the response of gastrointestinal stromal tumors after imatinib mesylate treatment: a quantitative analysis correlated with FDG PET findings. AJR Am J Roentgenol 2004;183:1619–28.
8. Golman K, Petersson JS. Metabolic imaging and other applications of hyperpolarized ^{13}C. Acad Radiol 2006;13: 932–42.
9. Gallagher F, Kettunen M, Brindle K. Biomedical applications of hyperpolarized ^{13}C magnetic resonance imaging. Prog NMR Spectrosc 2009;55:285–95.
10. Ardenkjaer-Larsen JH, Golman K, Brindle KM. Hyperpolarized ^{13}C magnetic resonance imaging: principles and applications. In: Weissleder R, Gambhir SS, Ross BD, Rehemtulla A, eds. Molecular imaging: principles and practice. Hamilton, Canada: BC Decker Inc.; 2009.
11. Viale A, Aime S. Current concepts on hyperpolarized molecules in MRI. Curr Opin Chem Biol 2011;14:90–6.
12. Kurhanewicz J, Vigneron D, Brindle K, Chekmenev E, Comment A, Cunningham C, et al. Analysis of cancer metabolism by imaging hyperpolarized nuclei: prospects for translation to clinical research. Neoplasia 2011;13:81–97.
13. Brindle KM, Bohndiek SE, Gallagher FA, Kettunen MI. Tumor imaging using hyperpolarized ^{13}C magnetic resonance spectroscopy. Magn Reson Med 2011;66:505–19.
14. Johnson GA, Benveniste H, Black RD, Hedlund LW, Maronpot RR, Smith BR. Histology by magnetic-resonance microscopy. Magn Reson Quart 1993;9:1–30.
15. Gadian DG, Radda GK. NMR studies of tissue metabolism. Annu Rev Biochem 1981;50:69–83.
16. Nelson SJ. Assessment of therapeutic response and treatment planning for brain tumors using metabolic and physiological MRI. NMR Biomed 2011;24:734–49.
17. Kurhanewicz J, Swanson MG, Nelson SJ, Vigneron DB. Combined magnetic resonance imaging and spectroscopic imaging approach to molecular imaging of prostate cancer. J Magn Reson Imaging 2002;16:451–63.
18. Kwock L, Smith JK, Castillo M, Ewend MG, Collichio F, Morris DE, et al. Clinical role of proton magnetic resonance spectroscopy in oncology: brain, breast, and prostate cancer. Lancet Oncol 2006;7:859–68.
19. Mayer D, Yen YF, Tropp J, Pfefferbaum A, Hurd RE, Spielman DM. Application of subsecond spiral chemical shift imaging to real-time multislice metabolic imaging of the rat *in vivo* after injection of hyperpolarized $^{13}C_1$-pyruvate. Magn Reson Med 2009;62:557–64.
20. Overhauser AW. Polarization of nuclei in metals. Phys Rev 1953;92:411–15.
21. Ardenkjaer-Larsen JH, Fridlund B, Gram A, Hansson G, Hansson L, Lerche MH, et al. Increase in signal-to-noise ratio of >10,000 times in liquid-state NMR. Proc Natl Acad Sci USA 2003;100:10158–63.
22. Allouche-Arnon H, Gamliel A, Barzilay C, Nalbandian R, Gomori J, Karlsson M, et al. A hyperpolarized choline molecular probe for monitoring acetylcholine synthesis. Contrast Media Mol Imaging 2011;6:139–47.
23. Qu WC, Zha ZH, Lieberman BP, Mancuso A, Stetz M, Rizzi R, et al. Facile synthesis [5-(13)C-4-(2)H(2)]-L-glutamine for hyperpolarized MRS imaging of cancer cell metabolism. Acad Radiol 2011;18:932–9.
24. Day SE, Kettunen MI, Gallagher FA, Hu DE, Lerche M, Wolber J, et al. Detecting tumor response to treatment using hyperpolarized ^{13}C magnetic resonance imaging and spectroscopy. Nat Med 2007;13:1382–7.
25. Ward CS, Venkatesh HS, Chaumeil MM, Brandes AH, Vancriekinge M, Dafni H, et al. Noninvasive detection of target modulation following phosphatidylinositol 3-kinase inhibition using hyperpolarized ^{13}C magnetic resonance spectroscopy. Cancer Res 2009;70:1296–305.
26. Schroeder MA, Cochlin LE, Heather LC, Clarke K, Radda GK, Tyler DJ. In vivo, assessment of pyruvate dehydrogenase flux in the heart using hyperpolarized carbon-13 magnetic resonance. Proc Natl Acad Sci USA 2008;105: 12051–6.
27. Merritt ME, Harrison C, Storey C, Jeffrey FM, Sherry AD, Malloy CR. Hyperpolarized ^{13}C allows a direct measure of flux through a single enzyme-catalyzed step by NMR. Proc Natl Acad Sci USA 2007;104:19773–7.
28. Chen AP, Kurhanewicz J, Bok R, Xua D, Joun D, Zhang V, et al. Feasibility of using hyperpolarized [1-^{13}C]lactate as a substrate for *in vivo* metabolic ^{13}C MRSI studies. Magn Reson Imaging 2008;26:721–6.
29. Witney TH, Kettunen MI, Brindle KM. Kinetic modeling of hyperpolarized ^{13}C label exchange between pyruvate and lactate in tumor cells. J Biol Chem 2011;286:24572–80.
30. Harris T, Eliyahu G, Frydman L, Degani H. Kinetics of hyperpolarized $^{13}C_1$-pyruvate transport and metabolism in living human breast cancer cells. Proc Natl Acad Sci USA 2009;106:18131–6.
31. Zierhut ML, Yen YF, Chen AP, Bok R, Albers MJ, Zhang V, et al. Kinetic modeling of hyperpolarized C-13(1)-pyruvate metabolism in normal rats and TRAMP mice. J Magn Reson 2009;202:85–92.
32. Kettunen MI, Hu D-E, Witney TH, McLaughlin R, Gallagher FA, Bohndiek SE, et al. Magnetization transfer measurements of exchange between hyperpolarized [1-^{13}C]pyruvate and [1-^{13}C]lactate in a murine lymphoma. Magn Reson Med 2010;63:872–80.
33. Bohndiek SE, Kettunen MI, Hu D-E, Witney TH, Kennedy BWC, Gallagher FA, et al. Detecting tumor response to a vascular disrupting agent using ^{13}C magnetic resonance spectroscopy and hyperpolarized [1-^{13}C]pyruvate and [1,4-$^{13}C_2$]fumarate. Mol Cancer Ther 2010;9:3278–88.
34. Vivanco I, Sawyers CL. The phosphatidylinositol 3-kinase-AKT pathway in human cancer. Nat Rev Cancer 2002;2: 489–501.
35. Brindle K. Metabolomics: Pandora's box or Aladdin's cave? Biochemist 2003;25:15–17.
36. Witney T, Kettunen M, Day S, Hu D, Neves A, Gallagher F, et al. A comparison between radiolabeled fluorodeoxyglucose uptake and hyperpolarized C-13-labeled pyruvate utilization as methods for detecting tumor response to treatment. Neoplasia 2009;6:574–82.
37. Albers MJ, Bok R, Chen AP, Cunningham CH, Zierhut ML, Zhang VY, et al. Hyperpolarized ^{13}C lactate, pyruvate, and alanine: noninvasive biomarkers for prostate cancer detection and grading. Cancer Res 2008;68:8607–15.
38. Park I, Larson PEZ, Zierhut ML, Hu S, Bok R, Ozawa T, et al. Hyperpolarized ^{13}C magnetic resonance metabolic imaging: application to brain tumors. Neurooncology 2010;12:133–44.
39. Day SE, Kettunen MI, Cherukuri MK, Mitchell JB, Lizak MJ, Morris HD, et al. Detecting response of rat C6 glioma tumors to radiotherapy using hyperpolarized [1-^{13}C]pyruvate and ^{13}C magnetic resonance spectroscopic imaging. Magn Reson Med 2011;65:557–63.
40. Nguyen QD, Smith G, Glaser M, Perumal M, Årstad E, Aboagye EO. Positron emission tomography imaging of drug-induced tumor apoptosis with a caspase-3/7 specific

[18F]-labeled isatin sulfonamide. Proc Natl Acad Sci USA 2009;106:16375–80.
41. Moffat BA, Chenevert TL, Lawrence TS, Meyer CR, Johnson TD, Dong Q, et al. Functional diffusion map: a noninvasive MRI biomarker for early stratification of clinical brain tumor response. Proc Natl Acad Sci USA 2005;102:5524–9.
42. Zhao M, Beauregard DA, Loizou L, Davletov B, Brindle KM. Non-invasive detection of apoptosis using magnetic resonance imaging and a targeted contrast agent. Nat Med 2001;7:1241–4.
43. Krishnan AS, Neves AA, de Backer MM, Hu D-E, Davletov B, Kettunen MI, et al. Detection of cell death in tumors using MRI and a gadolinium-based targeted contrast agent. Radiology 2008;246:854–62.
44. Canuto HC, McLachlan C, Kettunen MI, Velic M, Krishnan AS, Neves AA, et al. Characterization of image heterogeneity using 2D Minkowski functionals increases the sensitivity of detection of a targeted MRI contrast agent. Magn Reson Med 2009;61:1218–24.
45. Prescher JA, Contag CH. Guided by the light: visualizing biomolecular processes in living animals with bioluminescence. Curr Opin Chem Biol 14;80–9.
46. Weissleder R, Tung CH, Mahmood U, Bogdanov A. In vivo imaging of tumors with protease-activated near-infrared fluorescent probes. Nat Biotech 1999;17:375–8.
47. Gallagher FA, Kettunen MI, Hu DE, Jensen PR, in't Zandt R, Karlsson M, et al. Production of hyperpolarized [1,4-^{13}C)]malate from [1,4-^{13}C)]fumarate is a marker of cell necrosis and treatment response in tumors. Proc Natl Acad Sci USA 2009;106:19801–6.
48. Witney TH, Kettunen MI, Hu D-E, Gallagher FA, Bohndiek SE, Napolitano R, et al. Detecting treatment response in a model of human breast adenocarcinoma using hyperpolarised [1-^{13}C]pyruvate and [1,4-$^{13}C_2$]fumarate. Br J Cancer 2010;103:1400–6.
49. in't Zandt R. Metabolic reactions studied with 13C-DNP-MR in vitro and in vivo. Proc Int Soc Magn Reson Med 2008;16:827.
50. Kettunen M, Clatworthy M, Witney T, Hu D-E, Kennedy B, Bohndiek S, et al. Detection of acute kidney injury using hyperpolarized [1,4-$^{13}C_2$]fumarate. Proc Int Soc Magn Reson Med 2011;19:3513.
51. Cairns RA, Harris IS, Mak TW. Regulation of cancer cell metabolism. Nat Rev Cancer 2011;11:85–95.
52. Gao P, Tchernyshyov I, Chang TC, Lee YS, Kita K, Ochi T, et al. c-Myc suppression of miR-23a/b enhances mitochondrial glutaminase expression and glutamine metabolism. Nature 2009;458:762–5.
53. Gallagher F, Kettunen M, Day S, Lerche M, Brindle K. ^{13}C Magnetic resonance spectroscopy measurements of glutaminase activity in human hepatocellular carcinoma cells using hyperpolarized ^{13}C-labeled glutamine. Magn Reson Med 2008;60:253–7.
54. Shields AF, Grierson JR, Dohmen BM, Machula H-J, Stayanoff JC, Lawhorn-Crews JM, et al. Imaging proliferation *in vivo* with [F-18]FLT and positron emission tomography. Nature Med 1998;11:1334–6.
55. Vesselle H, Grierson J, Muzi M, Pugsley JM, Schmidt RA, Rabinowitz P, et al. *In vivo* validation of 3'deoxy-3'-[F-18]fluorothymidine ([F-18]FLT) as a proliferation imaging tracer in humans: correlation of [F-18]FLT uptake by positron emission tomography with Ki-67 immunohistochemistry and flow cytometry in human lung tumors. Clin Cancer Res 2002;8:3315–23.
56. Zhao SM, Lin Y, Xu W, Jiang WQ, Zha ZY, Wang P, et al. Glioma-derived mutations in IDH1 dominantly inhibit IDH1 catalytic activity and induce HIF-1 alpha. Science 2009;324:261–5.
57. Xu W, Yang H, Liu Y, Yang Y, Wang P, Kim SH, et al. Oncometabolite 2-hydroxyglutarate is a competitive inhibitor of alpha-ketoglutarate-dependent dioxygenases. Cancer Cell 2011;19:17–30.
58. Gallagher F, Kettunen M, Day S, Hu D-E, Karlsson M, Gisselsson A, et al. Detection of tumor glutamate metabolism in vivo using ^{13}C magnetic resonance spectroscopy and hyperpolarized [1-^{13}C]glutamate. Magn Reson Med 2011;66:18–23.
59. Gallagher F, Kettunen M, Day S, Hu D-E, Ardenkjær-Larsen J, in't Zandt R, et al. Magnetic resonance imaging of pH *in vivo* using hyperpolarized ^{13}C-labeled bicarbonate. Nature 2008;453:940–3.
60. Bohndiek SE, Kettunen MI, Hu D-E, Kennedy BWC, Boren J, Gallagher FA, et al. Hyperpolarized [1-^{13}C]-ascorbic and dehydroascorbic acid: vitamin C as a probe for imaging redox status in vivo. J Am Chem Soc 2011;133:11795–801.
61. Gillies RJ, Raghunand N, Garcia-Martin ML, Gatenby RA. pH imaging. A review of pH measurement methods and applications in cancers. IEEE Eng Med Biol Mag 2004;23:57–64.
62. Ardenkjaer-Larsen JH, Leach AM, Clarke N, Urbahn J, Anderson D, Skloss TW. Dynamic nuclear polarization polarizer for sterile use intent. NMR Biomed 2011;24:927–32.
63. Cunningham CH, Chen AP, Albers MJ, Kurhanewicz J, Hurd RE, Yen YF, et al. Double spin-echo sequence for rapid spectroscopic imaging of hyperpolarized ^{13}C. J Magn Reson 2007;187:357–62.
64. Yen YF, Kohler SJ, Chen AP, Tropp J, Bok R, Wolber J, et al. Imaging considerations for in vivo 13C metabolic mapping using hyperpolarized 13C-pyruvate. Magn Reson Med 2009;62:1–10.
65. Mayer D, Levin Y, Hurd R, Glover G, Spielman D. Fast metabolic imaging of systems with sparse spectra: application for hyperpolarized ^{13}C imaging. Magn Reson Med 2006;56:932–7.
66. Mayer D, Yen YF, Levin YS, Tropp J, Pfefferbaum A, Hurd RE, et al. In vivo application of sub-second spiral chemical shift imaging (CSI) to hyperpolarized ^{13}C metabolic imaging: comparison with phase-encoded CSI. J Magn Reson 2010;204:340–5.
67. Schulte R, Wiesinger F, Fish K, Whitt D, Hancu I. Efficient hyperpolarised ^{13}C metabolic imaging with rosette spectroscopic imaging. Proc Int Soc Magn Reson Med 2009;17:2433.
68. Valentin J. The 2007 recommendations of the International Commission on Radiological Protection. ICRP Publication no. 103. Ottawa, Canada: ICRP; 2007.
69. MacKenzie JD, Yen YF, Mayer D, Tropp JS, Hurd RE, Spielman DM. Detection of inflammatory arthritis by using hyperpolarized (13)C-pyruvate with MR imaging and spectroscopy. Radiology 2011;259:414–20.